Resonant Auger Decay in Benzene

Nayanthara K. Jayadev[a], Thomas-C. Jagau[b], and Anna I. Krylov[a]

[a] Department of Chemistry, University of Southern California, Los Angeles, CA 90089, USA

[b] Department of Chemistry, KU Leuven, B-3001 Leuven, Belgium

October 27, 2024

Abstract

We present *ab initio* calculations of the resonant Auger spectrum of benzene. In the resonant process, Auger decay ensues following the excitation of a core-level electron to a virtual orbital. Hence, resonant Auger decay manifests itself in the Auger spectrum by features with higher Auger electron energy compared to non-resonant decay. We apply equation-of-motion coupled-cluster (EOM-CC) methods to compute the spectrum in order to explain the main features in the experimental spectrum and to assess the capability and limitations of the available theoretical approaches. The results indicate that participator decay can be well described with the Feshbach–Fano approach based on EOM-CC wavefunctions in the singles and doubles (SD) approximation, but spectator decay is more difficult to describe. This is because the target states of spectator decay are doubly excited, resulting in the need to include triple excitations in the EOM-CC wave function. Resonant Auger decay in benzene is thus a challenging test case for EOM-CC theory. We examine the performance of different noniterative triple corrections to EOM-IP-CCSD and our numerical results highlight the need to include triple excitations iteratively.

1 Introduction

Auger decay is a non-radiative process in which a core-vacancy state decays by filling the hole and ejecting a second electron. It is a consequence of the metastable nature of highly energetic core-vacancy states located well above the ionization onset. Depending on whether the initial state is core-excited or core-ionized, one can distinguish between resonant and non-resonant

Auger decay, as illustrated in Fig. 1. In the former, the final states are singly ionized and in the latter doubly ionized.

Fig. 1 also shows that resonant Auger decay can be further classified as participator or spectator decay depending on whether the initially excited electron takes part in the decay. Regular Auger decay takes place when the excitation energy exceeds the core ionization energy whereas the resonant Auger process takes place when the excitation energy is below the ionization threshold of the respective core.

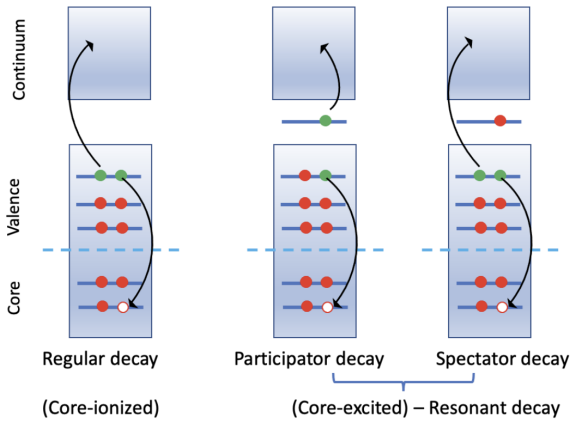

Figure 1: Different types of Auger decay.

Auger processes accompany many, if not all, X-ray induced processes.[1] Practical uses of Auger electrons include analytical techniques for surfaces,[2,3,4] materials,[5] nanostructures,[6,7,8] and molecules.[9,10,11,12] In addition, Auger electrons are also used for precision cancer treatments.[13,14,15,16,17] As with other spectroscopies, theoretical modeling helps to interpret the experimental spectra in terms of essential details of electronic structure. The positions of the peaks in an Auger spectrum are the energies of the Auger electrons, given by the energy differences between the initial core-hole state and the final states. The intensities of the individual peaks are proportional to the respective rates of decay, which are in turn proportional to the partial widths of the core-hole state. As per Fig. 1, participator decay should result in faster Auger electrons relative to non-resonant and spectator decay, while the spectator decay is expected to contribute to the lower-energy part of the Auger spectrum.

Ab initio calculations of Auger spectra are challenging because of the difficulties with computing core-vacancy states due to their metastable nature. Additional complications arise due to the large number of decay channels and the open-shell character of the final states.

In early theoretical work on molecular Auger decay, the decay rates were assumed to be identical for all target states of a given multiplicity.[18,19] The results indicated that for polyatomic

molecules, non-resonant Auger spectra could be reasonably well described by using the density of final states, provided that the contributions of triplet decay channels are scaled down relative to singlet channels.

Alternatively, decay rates can be computed explicitly. One possible technique is the Feshbach–Fano method in which the Hilbert space is partitioned into bound and continuum configurations.[20,21,22] The core-valence separation is commonly used to define the bound part of the Hilbert space.[23,24,25,26,27] For the treatment of the continuum part, a great variety of methods have been proposed. For example, Stieltjes imaging[28,29] was employed on top of the algebraic diagrammatic construction (ADC) approach[30] to evaluate partial widths, which were then normalized to sum up to the correct total width.[31,32] Recently, Kolorenc and Averbukh introduced the Fano-ADC(2,2) method,[33] which provides an improved description of the initial and final states, and is also useful for modeling double Auger decay.[34]

Whereas Stieltjes imaging treats the continuum wavefunctions implicitly, it is also possible to construct them explicitly, for example using the one-center approximation[35,36,37,38] or by solving a one-electron radial Schrödinger equation with spherical continuum wave functions.[39,40] Time-dependent studies of resonant Auger decay,[41] including the investigation of core-excited CO by Demekhin and Cederbaum,[42] are also noteworthy.

Recently, two new approaches for computing decay rates of core-hole states were introduced, one based on the Feshbach–Fano formalism[43] and another based on the complex basis function (CBF) method.[44,45,46,47] Both techniques were implemented using the equation-of-motion coupled-cluster (EOM-CC) ansatz[48] for describing initial core-hole and final valence-ionized states and tested on atoms and small molecules for which highly reliable partial decay widths and well-resolved Auger spectra are available.[49,46,47,50,51,52,53]

These two CC/EOM-CC based techniques were also applied to compute the non-resonant Auger spectrum of benzene,[54] resulting in a remarkable agreement between the two fundamentally different approaches for treating the continuum. The comparison with the experiment was less straightforward because three experimental studies[55,56,57] reported Auger spectra of benzene that did not align even after applying a global shift. However, the computations captured the general shape of the spectrum well, with differences of the same magnitude as the discrepancies between the experimental spectra.

In this contribution, we extend our study of Auger decay in benzene to the resonant process. Both resonant and non-resonant Auger spectra of benzene were reported by Rennie *et al.*, who measured absolute photoabsorption cross sections of benzene using synchrotron radiation.[56] Resonant and regular Auger spectra were measured at the main features of the photoabsorption

spectrum of benzene, including the $1s_C \rightarrow \pi^*$ resonance. Fig. 2 shows these experimental Auger spectra. As expected, the resonant spectrum features several higher-energy peaks relative to the non-resonant spectrum. We will discuss the experimental spectra in more detail below, after reviewing the electronic structure and the x-ray absorption spectrum (XAS) of benzene.

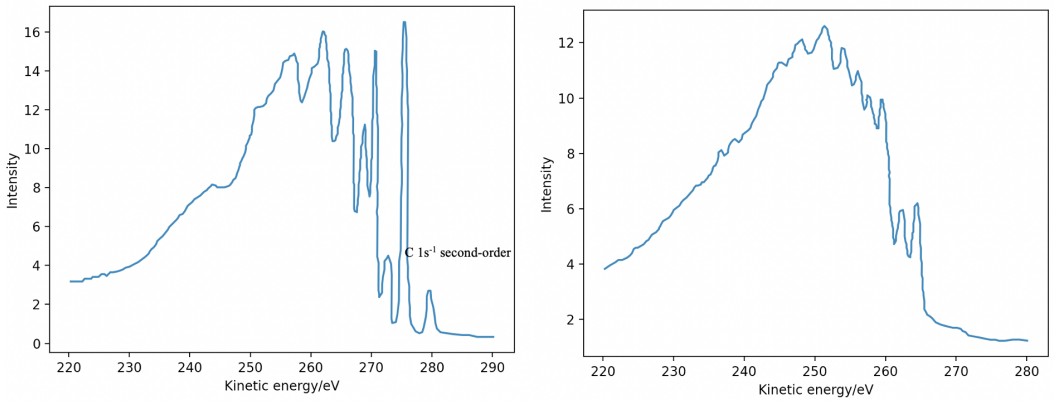

Figure 2: The Auger spectra of benzene measured at two different X-ray energies.[56] Left panel: 285 eV. Right panel: 390 eV (sudden limit).

The structure of the paper is as follows. Section 2 describes the computational methods. The numerical results and a comparison with the experiment are presented in Section 3. Our concluding remarks are given in Section 4.

2 Computational details

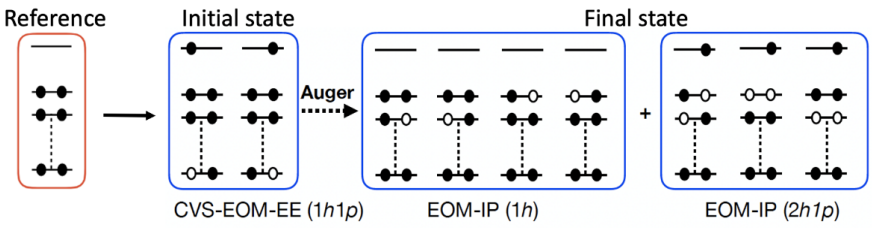

Figure 3: The initial and final states in resonant Auger decay can be computed with CVS-EOM-EE-CCSD and EOM-IP-CCSD, respectively.

The calculations were carried out at the equilibrium structure of benzene optimized with RI-MP2/cc-pVTZ; Cartesian coordinates are given in the SI. We computed the Auger spectrum using the Feshbach–Fano approach combined with EOM-CC wave functions in the singles and doubles approximation (EOM-CCSD) as devised by Skomorowski and Krylov.[43,49] The initial

states of the resonant Auger decay process, in which one core electron is excited to a virtual orbital, were computed using CVS-EOM-EE-CCSD using the frozen-core CVS (fc-CVS) framework.[25,26,27] The final states, i.e., the decay channels, were computed using EOM-IP-CCSD; the core electrons in the carbon K-shells were frozen in these calculations.

As shown in Fig. 3, in the case of participator and spectator decay the decay channels correspond to 1-hole (*1h*) and 2-hole-1-particle (*2h1p*) EOM-IP-CC states, respectively. This means that the spectator decay channels are not described well within the EOM-CCSD approximation. To account for triple excitations, we carried out EOM-IP-CCSD(fT)[58,59] and EOM-IP-CCSD(T)(a)* calculations.[60,61] In the former method, a correction to the EOM-CCSD energy is computed, whereas the latter method corrects the EOM-CC similarity-transformed Hamiltonian. In all EOM-CC calculations, the closed-shell ground state of benzene was used as the reference state.

The fully uncontracted 6-311(2+,+)G** basis set, denoted as u6-311(2+,+)G**, was used in all EOM-CCSD calculations.[62,63] We used the same basis set for EOM-IP-CCSD(fT) and EOM-IP-CCSD(T)(a)* calculations. However, due to convergence issues in the EOM-IP-CCSD(T)(a)* calculations, we were unable to compute a sufficient number of *2h1p* states. Thus, we carried out additional EOM-IP-CCSD(T)(a)* calculations for the missing states using the 6-311(+)G* basis.

The continuum orbital was treated as a plane wave in the calculations of the decay widths. The **k**-vector integration in these calculations was carried out using Lebedev quadrature. We note that calculations with the default grid of order 5 yield partial widths that break symmetry-imposed constraints.[54] Hence, we computed the resonant Auger spectrum of benzene with a tighter integration grid of order 17; the difference between the spectra obtained with the two grids is shown in the SI. The Auger spectra were generated from the computed energies and decay widths convoluted with a Gaussian function with a fixed full width at half maximum equal to 1.15 eV. All electronic structure calculations were carried out using the Q-Chem package.[64,65]

3 Results and discussions

3.1 Molecular orbitals of benzene

The molecular orbital (MO) diagram of benzene is shown in Fig. 4. Benzene belongs to the non-Abelian point group D_{6h}. Since most quantum chemistry packages, including Q-Chem, use Abelian subgroups, we use in the discussion below the irreducible representations of the

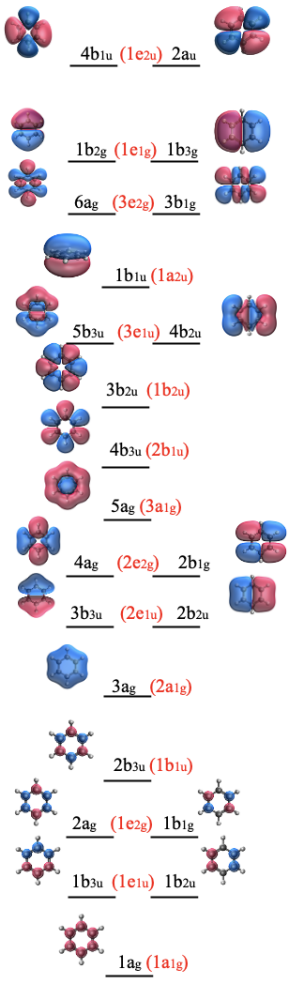

Figure 4: Molecular orbital diagram of benzene. Irreducible representations are given for the full point group D_{6h} (in red) using Mulliken's convention[66] and for the largest Abelian subgroup D_{2h} (in black) using Q-Chem's convention.[67] The $\pi*$-like $1e_{2u}$ orbitals represent the lowest unoccupied molecular orbital (LUMO) and are unoccupied in the ground state of benzene.

Abelian subgroup D_{2h} for the electronic states and MOs. The electronic configuration of the core electrons is

$$(1a_g)^2(1b_{3u})^2(1b_{2u})^2(2a_g)^2(1b_{1g})^2(2b_{3u})^2, \tag{1}$$

corresponding to the six $1s_C$ orbitals. The $1b_{3u}$ and $1b_{2u}$ orbitals as well as the $2a_g$ and $1b_{1g}$ orbitals are degenerate and form the $1e_{1u}$ and $1e_{2g}$ shells, respectively, in the full point group.

3.2 X-ray absorption spectrum of benzene

To understand the resonant Auger spectrum of benzene, we begin by reviewing its XAS spectrum. XAS probes core-excited states, which are the initial states of resonant Auger decay.

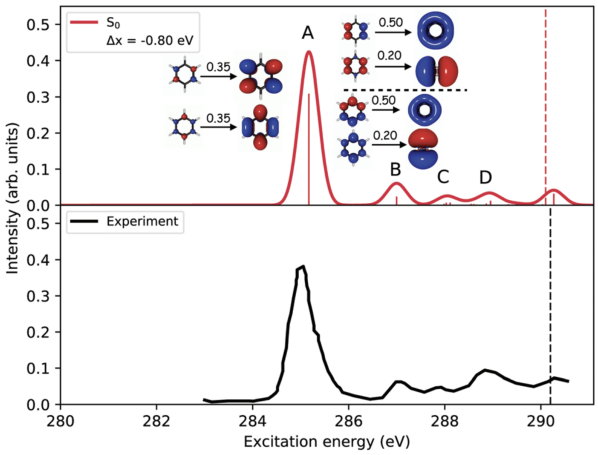

Figure 5: The XAS spectrum of benzene computed with CVS-EOM-EE-CCSD in the 6-311(2+,+)G** basis set with uncontracted carbon core. Reproduced with permission from Ref. 68.

Fig. 5 shows the XAS spectrum of benzene computed by Nanda *et al.*[68,69] The positions and relative intensities of the main peaks agree with the experimental spectrum after applying a redshift of 0.8 eV.

Fig. 5 also shows the leading natural transition orbitals (NTOs)[70,71] According to the NTOs, the peak A in the XAS spectrum originates from $1s_C \rightarrow \pi^*$ transitions and the doubly degenerate peak B originates from $1s_C \rightarrow Ry(\mathrm{B}_{2u}/\mathrm{B}_{3u})$ transitions. The NTO analysis further reveals that the excitations that give rise to peak A create a hole in the $1a_g$ and $1b_{1g}$ core orbitals, whereas the excitations that correspond to peak B create holes in the $1b_{2u}/1b_{3u}$ and in $1a_g$ orbitals

In the SI (Fig. S1 and Table S1) we show the XAS transitions that cover the relevant energy range as well as excitation energies and oscillator strengths computed with the fully uncontracted 6-311(2+,+)G** basis set. The results are similar to those computed in the partially uncontracted 6-311(2+,+)G** basis set used in Ref. 68).

As discussed in the introduction, we compare our results to the experimental spectra by Rennie *et al.*[56] (see Fig. 2). They reported the XAS of benzene in the range from 285 eV to beyond the $1s_C$ threshold at 290.42 eV. In agreement with other reported XAS of benzene,[72,73] the by far most prominent feature is the $1s_C \rightarrow \pi^*$ excitation at around 285 eV, which is termed peak A in Ref. 68.

Fig. 2 shows the Auger spectrum measured at 285 eV, where the $1s_C \rightarrow \pi^*$ resonance is located, as well as in sudden limit conditions at 390 eV, i.e., way above the ionization threshold.[56] The Auger spectrum measured at 390 eV corresponds to regular Auger decay,

which we discussed in Ref. 54. Here, we focus on the spectrum measured at 285 eV, which corresponds to resonant Auger decay following excitation to the $1s_C \rightarrow \pi^*$ state. This state, which we model as $^1B_{1u}$ state in the D_{2h} subgroup, is the initial state in our calculations of resonant Auger decay. For comparison, we also computed Auger spectra for decay of the $^1B_{2u}/^1B_{3u}$ state, which corresponds to peak B in the XAS. However, Rennie *et al.*[56] did not report experimental Auger spectra with excitation energy corresponding to peak B.

3.3 EOM-IP-CCSD calculations of the decay channels

Table 1 lists the ionization energies (IEs) of the lowest ionized states of benzene computed with EOM-IP-CCSD. The EOM-IP amplitudes clearly identify the decay channels as describing participator or spectator decay (see Fig. 3). The *1h* states, characterized by the large square norm of R_1, correspond to participator decay and the *2h1p* states, characterized by the large square norm of R_2, correspond to spectator decay.

According to Table 1, the *1h* states give rise to the lower IE part of the Auger spectrum, i.e., the part with higher Auger electron energy. The *2h1p* spectator decay channels, derived by the removal of a valence electron and an accompanying excitation to the LUMO, give rise to lower-energy Auger electrons. Table 1 shows several spectator decay channels in which two electrons are removed from higher-lying occupied orbitals and one is placed in a low-lying virtual orbital. The analysis of the wavefunction reveals the multiconfigurational character of the $2h1p$ states.

3.4 Resonant Auger decay widths

Table 2 and Table 3 show the Auger electron energies and partial widths of the major decay channels of the $^1B_{1u}$ and $^1B_{2u}/^1B_{3u}$ states of benzene computed with EOM-CCSD. The $^1B_{1u}$ state gives rise to larger decay widths relative to the $^1B_{2u}/^1B_{3u}$ states. Almost all participator decay channels ($1h$ channels) of the $^1B_{1u}$ state have substantial partial width above 1 meV, leading to faster decay and, consequently, a higher probability of decay of the metastable core-excited state into these channels. The partial decay widths of the spectator decay channels ($2h1p$ channels) are smaller. This may be attributed to the stronger Coulomb interaction of the valence electrons with the core; for example, for autoionizing Rydberg states, it is well established that weaker interaction with the molecular core results in lower decay width.[74,75,76] However, our results might also be affected by an insufficient description of the $2h1p$ states. Notably, our calculations identified a large number of spectator decay channels, such that their combined width is substantial.

Table 1: IEs and wavefunction composition in terms of the leading amplitudes of the lowest ionized states of benzene computed with EOM-IP-CCSD/u6-311(2+,+)G**. The square norms of R_1^2 and R_2^2 distinguish $1h$ and $2h1p$ states.

State	Energy (eV)	Composition	R_1^2	R_2^2
$^2B_{2g}$ [a]	9.23	$1b_{2g}^{-1}$ (0.97)	0.94	0.06
^2A_g [a]	12.12	$6a_g^{-1}$ (0.96)	0.93	0.07
$^2B_{1u}$	12.55	$1b_{1u}^{-1}$ (0.94)	0.90	0.10
$^2B_{2u}$ [a]	14.41	$4b_{2u}^{-1}$ (0.96)	0.92	0.08
$^2B_{2u}$	14.82	$3b_{2u}^{-1}$ (0.96)	0.91	0.09
$^2B_{3u}$	15.83	$4b_{3u}^{-1}$ (0.96)	0.90	0.10
^2A_g	17.38	$5a_g^{-1}$ (0.94)	0.89	0.11
^2A_g [a]	19.62	$4a_g^{-1}$ (0.92)	0.86	0.14
^2A_u [a]	17.56	$1b_{2g}^{-1}1b_{3g}^{-1}4b_{1u}^{1}$ (0.50), $1b_{2g}^{-1}1b_{3g}^{-1}6b_{1u}^{1}$ (0.23)	0.00	1.00
^2A_u [a]	18.10	$1b_{3g}^{-2}2a_u^{1}$ (0.66), $1b_{2g}^{-1}1b_{3g}^{-1}4b_{1u}^{1}$ (0.41)	0.00	1.00
^2A_u [a]	20.27	$1b_{2g}^{-2}2a_u^{1}$ (0.60), $1b_{2g}^{-1}1b_{3g}^{-1}4b_{1u}^{1}$ (0.43)	0.00	1.00
$^2B_{3g}$	19.88	$1b_{3g}^{-1}1b_{2g}^{-1}6b_{2g}^{1}$ (0.31), $1b_{3g}^{-1}1b_{1u}^{-1}4b_{1u}^{1}$ (0.29), $1b_{2g}^{-1}1b_{1u}^{-1}2a_u^{1}$ (0.29)	0.00	1.00
$^2B_{2g}$	20.00	$1b_{3g}^{-1}1b_{1u}^{-1}2a_u^{1}$ (0.36), $1b_{2g}^{-1}1b_{1u}^{-1}4b_{1u}^{1}$ (0.36)	0.00	1.00

[a] These states are twofold degenerate. The irreducible representations of the second states are B_{3g}, B_{1g}, B_{3u}, and B_{1u} for the B_{3g}, A_g, B_{2u}, and A_u states, respectively.

Previous investigations showed that the branching ratio between spectator and participator decay can vary significantly and is sensitive to the molecular electronic structure; for example, in CH_4 and CF_4 participator decay contributes no more than 6% to the total decay width,[77,78] whereas that number amounts to 21% for the C-edge of CO.[79] We thus cannot say with certainty whether the dominance of the participator channels in benzene found by our calculations is real or an artifact due to an insufficient description of the electronic structure.

3.5 Resonant Auger spectrum of benzene

Fig. 6 shows the contributions of *1h* states and *2h1p* states to the Auger spectrum based on the data in Table 2. This helps to anticipate the different character of the channels in different energy regimes. The higher Auger electron regime has contributions mostly from participator decay channels formed by the ionization of outer valence orbitals. As we move towards lower Auger electron energy, peaks that mostly stem from spectator decay appear. The spectator decay channels (*2h1p* channels) are not well described by EOM-IP-CCSD. Hence, we anticipate

Table 2: Auger electron energies (in eV) and partial decay widths (in meV) for the main channels in resonant Auger decay of the core-excited $^1B_{1u}$ state of benzene.[a]

Decay channel	Energy	Width	
$^2B_{2g}(1b_{2g}^{-1})$ [b]	276.60	1.34	Participator
$^2A_g(6a_g^{-1})$ [b]	273.71	1.07	Participator
$^2B_{2u}(3b_{2u}^{-1})$	271.01	1.33	Participator
$^2B_{3u}(4b_{3u}^{-1})$	270.00	1.18	Participator
$^2A_g(4a_g^{-1})$ [b]	266.21	1.76	Participator
$^2B_{2u}(1b_{2u}^{-1}, 1b_{2g}^{-1}6a_g^{-1}2a_u^1, 1b_{2g}^{-1}3b_{1g}^{-1}4b_{1u}^1)$ [b]	265.50	1.12	Spectator
$^2B_{1u}(1b_{3g}^{-1}1b_{2g}^{-1}2a_u^1, 1b_{2g}^{-2}4b_{1u}^1, 1b_{3g}^{-2}4b_{1u}^1)$	264.21	0.75	Spectator
$^2B_{2g}(1b_{2g}^{-1}1b_{1u}^{-1}4b_{1u}^1, 1b_{3g}^{-1}1b_{1u}^{-1}2a_u^1)$	263.21	0.58	Spectator

[a] The partial decay widths were computed using a fine integration grid of order 17. [b] These states are twofold degenerate. The irreducible representations of the second states are B_{3g}, B_{1g}, and B_{3u} for the B_{2g}, A_g, and B_{2u} states, respectively.

that this part of the spectrum is not well described and that some account of triple excitations is needed for these states.

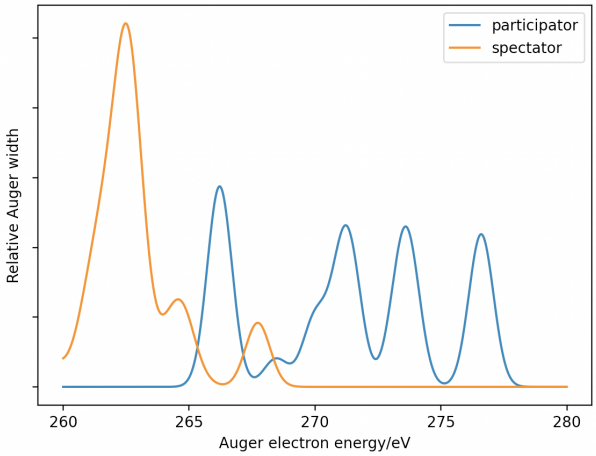

Figure 6: Contributions from participator and spectator decay channels to the resonant Auger spectrum of the core-excited $^1B_{1u}$ state of benzene at 285.83 eV.

Fig. 7 shows the theoretical Auger spectrum of the $^1B_{1u}$ core-excited state at 285.83 eV compared with the experimental spectrum[56] taken around the $1s_C \rightarrow \pi^*$ resonance at 285 eV. The peaks in the theoretical spectrum above 270 eV appear exclusively due to participator decay, and their positions agree well with the experimental spectrum. The peaks between 270 and 265 eV have contributions from both participator and spectator decay channels, whereas

Table 3: Auger electron energies (in eV) and partial decay widths (in meV) for the main channels in resonant Auger decay of the core-excited $^1B_{2u}$ and $^1B_{3u}$ states of benzene.[a]

Decay channel	Energy	Width	
$^2B_{2g}(1b_{2g}^{-1})^b$	278.43	0.64	Participator
$^2A_g(6a_g^{-1})^b$	275.54	0.47	Participator[c]
$^2B_{3u}(4b_{3u}^{-1})^b$	273.25	0.70	Participator
$^2B_{2u}(3b_{2u}^{-1})^b$	272.85	0.59	Participator
$^2B_{2u}(3b_{2u}^{-1})^b$	272.85	0.59	Participator
$^2A_g(1b_{2g}^{-2}13a_g^1, 1b_{3g}^{-2}13a_g^1, 1b_{2g}^{-2}9a_g^1, 1b_{3g}^{-2}9a_g^1)^b$	264.69	0.32	Spectator
$^2B_{1g}(1b_{3g}^{-1}1b_{2g}^{-1}13a_g^1, 1b_{3g}^{-1}1b_{2g}^{-1}9a_g^1)$	264.50	0.52	Spectator
$^2B_{2u}(2b_{2u}^{-1}, 1b_{2g}^{-1}6a_g^{-1}2a_u^1, 1b_{2g}^{-1}3b_{1g}^{-1}4b_{1u}^1)$	264.34	0.35	Spectator
$^2B_{2u}(1b_{3g}^{-2}8b_{2u}^1, 1b_{3g}^{-2}5b_{2u}^1, 1b_{3g}^{-2}7b_{2u}^1, 1b_{3g}^{-2}10b_{2u}^1)$	263.55	0.52	Spectator
$^2A_u(3b_{1g}^{-1}1b_{3g}^{-1}8b_{2u}^1, 3b_{1g}^{-1}1b_{3g}^{-1}10b_{2u}^1)$	261.65	0.34	Spectator
$^2A_g(1b_{2g}^{-2}13a_g^1, 1b_{3g}^{-2}13a_g^1, 1b_{2g}^{-2}9a_g^1, 1b_{3g}^{-2}9a_g^1)$	264.50	0.52	Spectator
$^2B_{3u}(3b_{3u}^{-1}, 1b_{3g}^{-1}3b_{1g}^{-1}4b_{1u}^1, 1b_{3g}^{-1}6a_g^{-1}2a_u^1)$	264.34	0.34	Spectator
$^2B_{2g}(1b_{2g}^{-1}6a_g^{-1}1a_g^1, 1b_{3g}^{-1}3b_{1g}^{-1}11a_g^1)$	262.16	0.30	Spectator
$^2B_{1u}(6a_g^{-1}1b_{2g}^{-1}9b_{3u}^1, 6a_g^{-1}1b_{2g}^{-1}11b_{3u}^1)$	261.65	0.34	Spectator

[a] The partial decay widths were computed using a fine integration grid of order 17.

[b] The decay channels are two-fold degenerate. Similarly, core-excited states $^1B_{2u}$ and $^1B_{3u}$, are also degenerate.

[c]The $^2A_g(6a_g^{-1})$ and $^2B_{1g}(3b_{1g}^{-1})$ decay channels are degenerate. However, the calculation yields different partial widths, either due to numeric issues or artefacts using Abelian subgroups. We report the averaged decay widths for these channels.

the remaining peaks with Auger electron energies below 265 eV arise exclusively from spectator decay. The agreement between theory and experiment in terms of the position and intensity of the peaks is rather poor in this energy range. This can be attributed to the poor description of $2h1p$ states by EOM-IP CCSD.

Fig. 7 also shows a spectrum in which an empirical redshift of +6.00 eV is applied to the Auger electron energy of all spectator decay channels to maximize the alignment. We note that 6 eV is a rather substantial redshift of the IEs. In the SI (Fig. S2), we show spectra with other redshifts; these do not align better.

After applying the global 6 eV shift, the theoretical spectrum aligns better with the experiment, both in terms of the number of peaks and their positions, but substantial disagreement

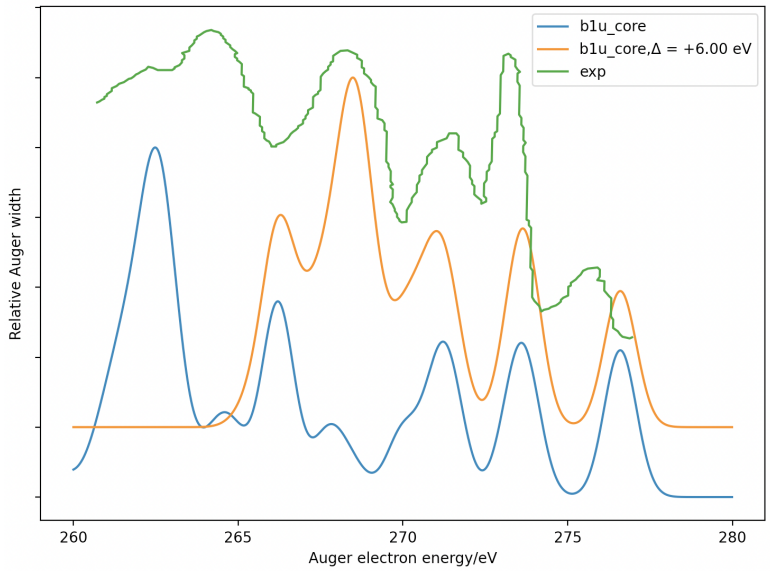

Figure 7: The computed resonant Auger spectrum for the core-excited $^1B_{1u}$ state at 285.83 eV along with the experimental spectrum by Rennie *et al.*[56] A spectrum in which the energies of all $2h1p$ channels are shifted by 6.00 eV to higher energy is also shown.

persists. Inclusion of triple excitations, which shifts each peak by a different energy, is clearly needed to improve the description of $2h1p$ states and their signatures in the Auger spectrum.

To better understand the effect of the initially excited state, we also computed the resonant Auger spectrum of the B_{2u}/B_{3u} core-excited state. Fig. 8 compares the spectra of the B_{1u} and B_{2u}/B_{3u} states; the experimental spectrum is also shown. We observe that the B_{1u} and B_{2u}/B_{3u} spectra are noticeably different. As anticipated, the B_{1u} spectrum matches the experimental spectrum much better. However, it is not clear whether the experimental spectrum also contains contributions from the B_{2u}/B_{3u} state due to insufficient spectral resolution. If this is the case, these additional contributions could explain the observed discrepancies between theory and experiment, for example, the peak at around 273 eV in the experimental spectrum.

3.6 Improving the description of the decay channels by including triples corrections

Table 4 presents the IEs of the decay channels computed using two different noniterative methods for the approximate treatment of triple excitations on top of EOM-CCSD, namely EOM-IP-CCSD(T)(a)* and EOM-IP-CCSD(fT). In the case of $1h$ states, the effect of the triples correction is less than 0.5 eV. Fig. 9 shows the participator decay spectrum of the core-excited B_{1u} and B_{2u}/B_{3u} states obtained from EOM-IP-CCSD and EOM-CCSD(T)(a)* calculations.

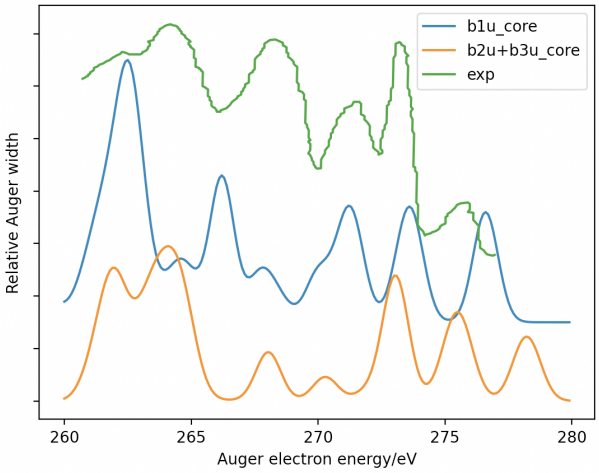

Figure 8: Theoretical Auger spectrum of the core-excited B_{1u} and B_{2u}/B_{3u} states compared with the spectrum measured by Rennie *et al.*[56] at 285 eV.

It is evident that the participator decay channels are well described at the EOM-IP-CCSD level of theory.

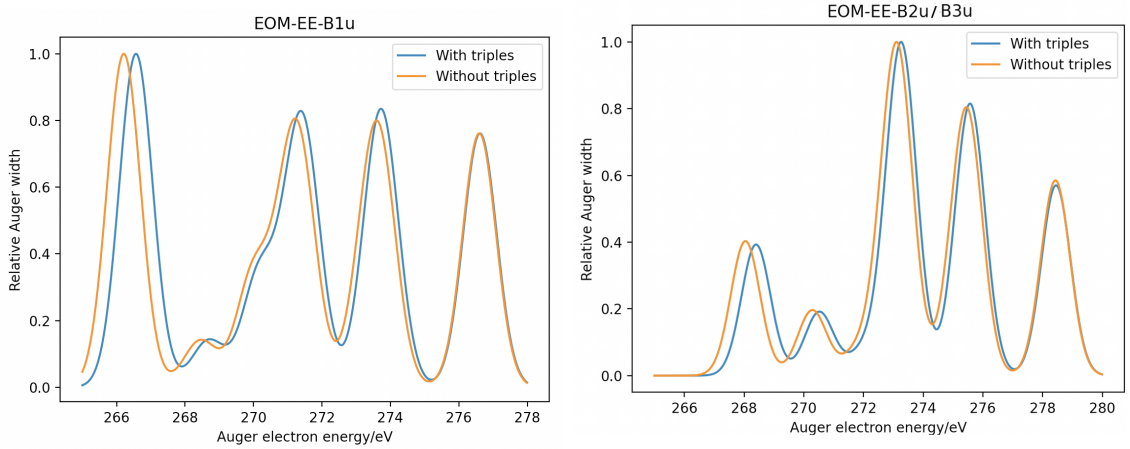

Figure 9: The participator decay Auger spectrum computed using EOM-IP-CCSD and EOM-IP-CCSD(T)(a)* for the decay channels. (a) $^1B_{1u}$ state, (b) $^1B_{2u}$/ $^1B_{3u}$ state.

As expected, the magnitude of the triples correction is much larger for the spectator decay channels, that is, the *2h1p* states, ranging between 3 and 6 eV. We were not able to compute all required *2h1p* states with EOM-CCSD(T)(a)*, but we were able to compute the correction for all spectator decay channels with EOM-CCSD(fT). Fig. 10 shows the total resonant Auger spectrum of the $^1B_{1u}$ state computed with and without the (fT) correction. The improvement in the relative position of the peaks due to the (fT) correction is clearly visible, but there is a stark disparity between experiment and theory in the intensity of the peak around 275 eV. As we expect participator decay to be more important than spectator decay in this energy

Table 4: Ionization energies of the lowest ionized states of benzene computed with different EOM-IP-CC methods. Absolute ionization energies are given for EOM-IP-CCSD and corrections relative to EOM-IP-CCSD for EOM-IP-CCSD(T)(a)* and EOM-IP-CCSD(fT).

State	EOM-CCSD	(T)(a)* [a]	(T)(a)* [b]	(fT)
$^2B_{2g}/^2B_{3g}$	9.23	-0.06	-0.02	-0.23
$^2A_g/^2B_{1g}$	12.12	-0.12	-0.10	-0.19
$^2B_{1u}$	12.55	-0.38	-0.24	-0.34
$^2B_{2u}/^2B_{3u}$	14.41	-0.14	-0.13	-0.20
$^2B_{2u}$	14.82	-0.22	-0.21	-0.30
$^2B_{3u}$	15.83	-0.18	-0.17	-0.21
^2A_g	17.38	-0.25	-0.24	-0.27
$^2A_g/^2B_{1g}$	19.62	-0.36	-0.36	-0.38
$^2A_u/^2B_{1u}$	17.56	-3.36	-3.04	-3.60
$^2A_u/^2B_{1u}$	18.10	-5.01	-3.42	-3.43
$^2A_u/^2B_{1u}$	20.27	-5.42	-5.09	-4.94
$^2B_{3g}$	19.88	-5.37	-	-3.10
$^2B_{2g}$	20.00	-5.14	-	-3.37
$^2B_{2u}/^2B_{3u}$	20.55	-4.26	-	-3.94
$^2B_{1u}$	21.61	-4.61	-	-5.65

[a] Computed in the 6-311(+)G* basis.

[b] Computed in the u6-311(2+,+)G** basis.

EOM-IP-CCSD and EOM-IP-CCSD(fT) calculations were carried out in the u6-311(2+,+)G** basis.

range, the discrepancy might be due to contributions of other core-excited states such as the $^1B_{2u}/^1B_{3u}$ state.

Table 4 compares the IEs computed with EOM-CCSD and EOM-CCSD(T)(a)* in the smaller 6-311(+)G* basis set. With this smaller basis set, we could calculate a larger number of spectator decay channels. Similar to the calculations in the larger basis set, the triples correction for spectator decay channels ranges between 3-6 eV.

Fig. S9 in the SI compares the spectra computed with EOM-CCSD and with inclusion of triples correction. Here, we shifted the EOM-IP-CCSD energies calculated in the u6-311(2+,+)G** basis using the EOM-IP-CCSD(T)(a)* triples correction calculated in the smaller 6-311(+)G* basis. We note that the (fT) and (T)(a)* corrections computed with a

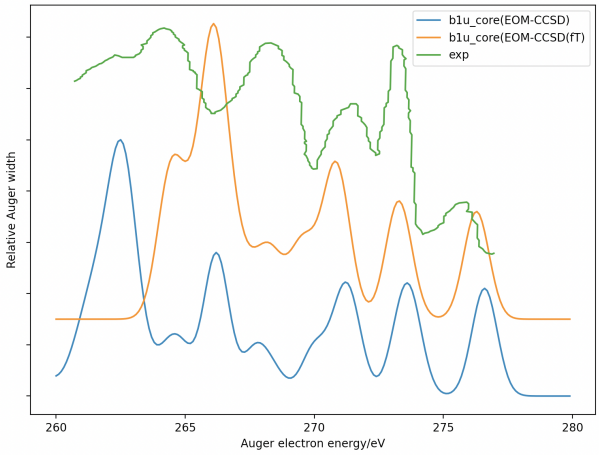

Figure 10: The resonant Auger spectrum of the core-excited $^1B_{1u}$ state computed using EOM-IP-CCSD and EOM-CCSD(fT) for the decay channels.

smaller basis are similar in magnitude.

From this analysis, it is clear that the effect of triple excitations on the $2h1p$ states can indeed reach a magnitude of 6 eV. With such a large correction, the accuracy of a perturbative treatment becomes questionable. Hence, for the reliable modeling of resonant Auger spectra, inclusion of triple excitations in an iterative fashion might be necessary.

3.7 Describing the spectator decay channels with EOM-DIP-CCSD

Anticipating the poor description of the $2h1p$ states by EOM-IP-CCSD, we also carried out EOM-DIP-CCSD calculations. The energies of the $2h$ states, shifted by the lowest $\pi\pi^*$ singlet excitation energy, which amounts to 5.21 eV computed with EOM-EE-CCSD ($^1B_{2u}$), can provide estimates for the IEs of the $2h1p$ states, assuming that the excited spectator electron is relatively far away and interacts only weakly with the molecular core.[80] We expect that such estimate provides an upped bound to the $2h1p$ EOM-IP states.

The comparison between the $2h$ EOM-DIP-CCSD states and the $2h1p$ EOM-IP-CCSD states is shown in Table 5. As one can see, the DIP states follow the same ordering as IP states, with their shifted energies being $\sim$2 eV higher. Hence, one can use DIP calculations to represent $2h1p$ IP states, but an additional empirical shift is needed to match the energies.

3.8 Natural Auger orbitals

To better understand the contributions of resonant decay to the Auger spectrum of benzene, we computed natural Auger orbitals (NAOs)[81] for different core-excited states and decay channels.

Table 5: Comparison between EOM-IP-CCSD energies of $2h1p$ states and EOM-DIP-CCSD energies of $2h$ states. The u6-311(2+,+)G** basis was used in all calculations. States are matched by their $2h$ configurations. All values in eV.

State	EOM-IP-CCSD	EOM-DIP-CCSD	EOM-DIP-CCSD, shifted[a]
$^2A_u/^2B_{1u}$	17.56	24.85	19.64
$^2A_u/^2B_{1u}$	18.10	25.48	20.27
$^2A_u/^2B_{1u}$	20.27	25.92	20.71
$^2B_{3g}$	19.88	25.48	20.27
$^2B_{2g}$	20.00	27.90	22.69

[a] EOM-DIP-CCSD energy minus lowest $\pi\pi^*$ singlet excitation energy of benzene computed with EOM-EE-CCSD/u6-311(2+,+)G**.

Fig. 11 shows the participator decay NAOs for the B_{1u}, and B_{2u} core-excited states.

NAOs provide information about the initial core-excited state and the final decay channels, which are the $1h$ states in the case of participator decay. Thus, NAOs are useful for examining the orbital picture associated with each decay channel. For instance, from Fig. 11, it is evident that the decay of the B_{1u} core-excited state creates a hole in the $2a_g$ and $1b_{1g}$ core orbitals of carbon. The initially excited electron populates the one of the LUMOs ($1b_{2g}$ or $1b_{3g}$) , which, in turn, takes part in resonant Auger decay, thereby ejecting the Auger electron from the corresponding HOMOs of benzene ($1b_{2g}$ and $1b_{3g}$). The degenerate $^1B_{2u}/^1B_{3u}$ core-excited states generate holes in the $1b_{2u}/1b_{3u}$ orbitals and in $1a_g/2a_g$ orbitals. Fig. 11 indeed shows that the B_{2u} core excitation corresponds to a $1s_c$ to Rydberg orbitals transition and the removal of the Auger electron from the $6a_g$ orbital (HOMO-1).

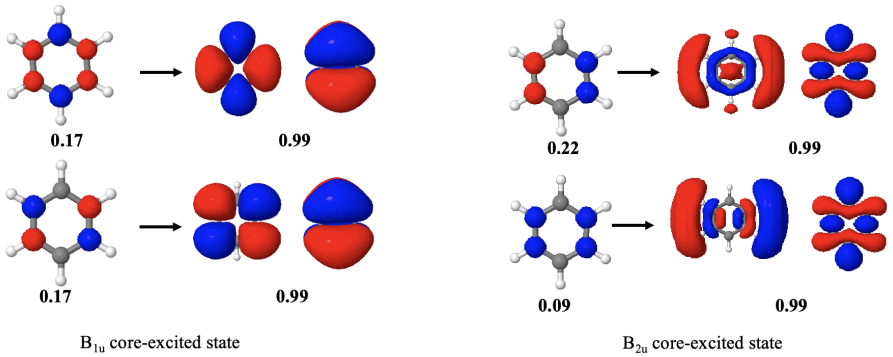

Figure 11: Natural Auger orbitals for participator Auger decay in benzene. Left: Decay of the core-excited $^1B_{1u}$ state into the $^2B_{1g}$ state. Right: Decay of the core-excited $^1B_{2u}$ state into the ^2A_g state.

4 Conclusions

We presented calculations of the resonant Auger decay spectrum of benzene using the Feshbach–Fano approach combined with EOM-CCSD wavefunctions and a description of the Auger electron in terms of plane waves. The calculations reproduce well the higher-energy part of the experimental Auger spectrum, which is dominated by participator decay. The lower-energy part of the spectrum, which includes contributions from spectator decay, shows large discrepancies with experiment.

This shortcoming is anticipated because the spectator decay channels are dominated by $2h1p$ configurations that are not well described by EOM-IP-CCSD. To improve the description of this part of the spectrum, we investigated several approaches: an empirical redshift of all $2h1p$ states by 6 eV, two types of noniterative triples corrections on top of EOM-IP-CCSD, as well as using EOM-DIP-CCSD energies shifted by the lowest $\pi\pi^*$ excitation energy of benzene. The so-corrected spectra agree better with experiment, but discrepancies still persist. The two triples corrections are in good agreement with each other; however, given the large magnitude of the correction of up to 6 eV, one may expect that a perturbative noniterative treatment is not sufficient and that an iterative inclusion of triple excitations is needed instead.

Furthermore, the triples corrections only affect the peak positions, whereas the decay widths are still computed based on EOM-IP-CCSD and EOM-DIP-CCSD wavefunctions. One may anticipate non-trivial effects of triple excitations on the decay width, which can affect the spectrum. It is also not clear whether the available experiment can reliably isolate the spectra arising from resonant Auger decay of different core-excited states. The X-ray absorption spectrum of benzene is dominated by a $1s_C \rightarrow \pi^*$ transition at 285 eV, but there are further core-excited states just a few electron-volts higher. Our results show that the Auger spectra resulting from excitations to the two lowest-lying peaks in the X-ray absorption spectrum are different, meaning that one may anticipate considerable changes in the resonant Auger spectrum if the two peaks are not spectrally resolved. Finally, given the large discrepancies between different experimental non-resonant Auger spectra of benzene,[54] one cannot rule out the possibility that the experimental resonant spectrum might be affected by some artifacts.

Acknowledgments

This work was supported in Los Angeles by the U.S. National Science Foundation (No. CHE-1856342 to A.I.K.) and in Leuven by the European Research Council (ERC) under the European

Union's Horizon 2020 research and innovation program (Grant No. 851766 to T.C.J.) and by the KU Leuven internal funds (Grant No. C14/22/083 to T.C.J.).

Conflicts of interest

The authors declare the following competing financial interest(s): A.I.K. is the president and a part-owner of Q-Chem, Inc.

Data availability

The data that support the findings of this study are available within the article and the associated SI.

References

[1] B. K. Agarwal, *X-ray spectroscopy: an introduction*, volume 15. Springer, 2013.

[2] T. Orvis, M. Surendran, Y. Liu, A. Cunniff, and J. Ravichandran, In situ Auger electron spectroscopy of complex oxide surfaces grown by pulsed laser deposition, J. Vac. Sci. Technol., A **37**, 061401 (2019).

[3] P. Weightman, X-ray-excited Auger and photoelectron spectroscopy, Electronic Properties of Surfaces , 135 (2018).

[4] Z. Li and U. Becker, Chemical state effects on the Auger transitions in Cr, Fe, and Cu compounds, J. Electron. Spectrosc. and Relat. Phenom. **237**, 146893 (2019).

[5] S. Hofmann, *Auger-and X-ray photoelectron spectroscopy in materials science: a user-oriented guide*, volume 49. Springer Science & Business Media, 2012.

[6] L.-C. Chao and S.-H. Yang, Growth and Auger electron spectroscopy characterization of donut-shaped ZnO nanostructures, Appl. Surf. Sci. **253**, 7162 (2007).

[7] S. N. Raman, D. F. Paul, J. S. Hammond, and K. D. Bomben, Auger electron spectroscopy and its application to nanotechnology, Microscopy today **19**, 12 (2011).

[8] W.E.S. Unger, T. Wirth, and V.-D. Hodoroaba, *Characterization of Nanoparticles*, chapter Chapter 4.3.2 - Auger electron spectroscopy, pages 373–395. Elsevier, 2020.

[9] R. R. Rye and J. E. Houston, Molecular auger spectroscopy, Acc. Chem. Res. **17**, 41 (1984).

[10] B. K. McFarland, J. P. Farrell, S. Miyabe, F. Tarantelli, A. Aguilar, N. Berrah, C. Bostedt, J. D. Bozek, P. H. Bucksbaum, J. C. Castagna, R. N. Coffee, J. P. Cryan, L. Fang, R. Feifel, K. J. Gaffney, J. M. Glownia, T. J. Martinez, M. Mucke, B. Murphy, A. Natan, T. Osipov, V. S. Petrović, S. Schorb, Th. Schultz, L. S. Spector, M. Swiggers, I. Tenney, S. Wang, J. L. White, W. White, and M. Gühr, Ultrafast x-ray Auger probing of photoexcited molecular dynamics, Nat. Comm. **5**, 4235 (2014).

[11] T. Marchenko, L. Inhester, G. Goldsztejn, O. Travnikova, L. Journel, R. Guillemin, I. Ismail, D. Koulentianos, D. Céolin, R. Püttner, M. N. Piancastelli, and M. Simon, Ultrafast nuclear dynamics in the doubly-core-ionized water molecule observed via Auger spectroscopy, Phys. Rev. A **98**, 063403 (2018).

[12] O. Plekan, H. Sa'adeh, A. Ciavardini, C. Callegari, G. Cautero, C. Dri, M. Di Fraia, K. C. Prince, R. Richter, R. Sergo, L. Stebel, M. Devetta, D. Faccialá, C. Vozzi, L. Avaldi, P. Bolognesi, M. C. Castrovilli, D. Catone, M. Coreno, F. Zuccaro, E. Bernes, G. Fronzoni, and D. Toffoli and A. Ponzi, Experimental and theoretical photoemission study of indole and its derivatives in the gas phase, J. Phys. Chem. A **124**, 4115 (2020).

[13] A. Ku, V. J. Facca, Z. Cai, and R. M. Reilly, Auger electrons for cancer therapy—a review, EJNMMI Radiopharm. Chem. **4**, 27 (2019).

[14] G. Pirovano, S. A. Jannetti, L. M. Carter, A. Sadique, S. Kossatz, N. Guru, P. Demétrio De Souza França, M. Maeda, B. M. Zeglis, J. S. Lewis, J. L. Humm, and T. Reiner, Targeted brain tumor radiotherapy using an Auger emitter, Clin. Cancer Res. **26**, 2871 (2020).

[15] J. Borbinha, P. Vaz, and S. Di Maria, Dosimetric assessment in different tumour phenotypes with Auger electron emitting radionuclides: ^{99m}Tc, ^{125}I, ^{161}Tb, and ^{177}Lu, Radiat. Phys. Chem. **172**, 108763 (2020).

[16] G. Pirovano, T. C. Wilson, and T. Reiner, Auger: The future of precision medicine, Nucl. Med. and Bio. **96**, 50 (2021).

[17] A. I. Kassis, The amazing world of Auger electrons, Int. J. Radiat. Bio. **80**, 789 (2004).

[18] F. Tarantelli, A. Sgamellotti, L. S. Cederbaum, and J. Schirmer, Theoretical investigation of many dicationic states and the Auger spectrum of benzene, J. Chem. Phys. **86**, 2201 (1987).

[19] E.M.-L. Ohrendorff, F. Tarantelli, and L.S. Cederbaum, Dicationic states of hydrocarbons and a statistical approach to their Auger spectra, J. Chem. Phys. **92**, 2984 (1990).

[20] U. Fano, Effects of configuration interaction on intensities and phase shifts, Phys. Rev. **124**, 1866 (1961).

[21] H. Feshbach, A unified theory of nuclear reactions. 2, Ann. Phys. (N.Y.) **19**, 287 (1962).

[22] P.-O. Löwdin, Studies in perturbation theory. IV. Solution of eigenvalue problem by projection operator formalism, J. Math. Phys. **3**, 969 (1962).

[23] L. S. Cederbaum, W. Domcke, and J. Schirmer, Many-body theory of core holes, Phys. Rev. A **22**, 206 (1980).

[24] S. Coriani and H. Koch, Communication: X-ray absorption spectra and core-ionization potentials within a core-valence separated coupled cluster framework, J. Chem. Phys. **143**, 181103 (2015).

[25] M. L. Vidal, X. Feng, E. Epifanovsky, A. I. Krylov, and S. Coriani, A new and efficient equation-of-motion coupled-cluster framework for core-excited and core-ionized states, J. Chem. Theory Comput. **15**, 3117 (2019).

[26] M. L. Vidal, A. I. Krylov, and S. Coriani, Dyson orbitals within the fc-CVS-EOM-CCSD framework: theory and application to X-ray photoelectron spectroscopy of ground and excited states, Phys. Chem. Chem. Phys. **22**, 2693 (2020).

[27] M. L. Vidal, A. I. Krylov, and S. Coriani, Correction to: "Dyson orbitals within the fc-CVS-EOM-CCSD framework: theory and application to X-ray photoelectron spectroscopy of ground and excited states", Phys. Chem. Chem. Phys. **22**, 3744 (2020).

[28] C.-M. Liegener, Green's function calculations on the Auger spectra of CO, Chem. Phys. Lett. **106**, 201 (1984).

[29] V. Carravetta and H. Ågren, Stieltjes imaging method for molecular Auger transition rates: Application to the Auger spectrum of water, Phys. Rev. A **35**, 1022 (1987).

[30] A. Dreuw and M. Wormit, The algebraic diagrammatic construction scheme for the polarization propagator for the calculation of excited states, WIREs: Comput. Mol. Sci. **5**, 82 (2015).

[31] V. Averbukh and L.S. Cederbaum, Ab initio calculation of interatomic decay rates by a combination of the Fano ansatz, Green's-function methods, and the Stieltjes imaging technique, J. Chem. Phys. **123**, 204107 (2005).

[32] S. Kopelke, K. Gokhberg, L. S. Cederbaum, F. Tarantelli, and V. Averbukh, Autoionization widths by Stieltjes imaging applied to Lanczos pseudospectra, J. Chem. Phys. **134**, 024106 (2011).

[33] P. Kolorenč and V. Averbukh, Fano-ADC(2,2) method for electronic decay rates, J. Chem. Phys. **152**, 214107 (2020).

[34] P. Kolorenč, Ab initio calculations of molecular double Auger decay rates, arXiv:2407.07426, 2024.

[35] H. Siegbahn, L. Asplund, and P. Kelfve, The Auger electron spectrum of water vapour, Chem. Phys. Lett. **35**, 330 (1975).

[36] R. F. Fink, M. N. Piancastelli, A. N. Grum-Grzhimailo, and K. Ueda, Angular distribution of Auger electrons from fixed-in-space and rotating C $1s \rightarrow 2\pi$ photoexcited CO: Theory, J. Chem. Phys. **130**, 014306 (2009).

[37] G. Grell and S. I. Bokarev, Multi-reference protocol for (auto) ionization spectra: Application to molecules, J. Chem. Phys. **152**, 074108 (2020).

[38] B. N. Cabral Tenorio, T. A. Voß, S. I. Bokarev, P. Decleva, and S. Coriani, Multi-reference approach to normal and resonant Auger spectra based on the one-center approximation, J. Chem. Theory Comput. **18**, 4387 (2022).

[39] G. Grell, O. Kühn, and S. I. Bokarev, Multireference quantum chemistry protocol for simulating autoionization spectra: Test of ionization continuum models for the neon atom, Phys. Rev. A **100**, 042512 (2019).

[40] L. Inhester, C. F. Burmeister, G. Groenhof, and H. Grubmüller, Auger spectrum of a water molecule after single and double core ionization, J. Chem. Phys. **136**, 144304 (2012).

[41] P. V. Demekhin and L. S. Cederbaum, Strong interference effects in the resonant Auger decay of atoms induced by intense x-ray fields, Phys. Rev. A **83**, 023422 (2011).

[42] P. V. Demekhin and L. S. Cederbaum, Resonant Auger decay of core-excited CO molecules in intense x-ray laser pulses: the O(1s$\rightarrow \pi^*$) excitation, J. Phys. B **46**, 164008 (2013).

[43] W. Skomorowski and A. I. Krylov, Feshbach-Fano approach for calculation of Auger decay rates using equation-of-motion coupled-cluster wave functions. I. Theory and implementation, J. Chem. Phys. **154**, 084124 (2021).

[44] T. N. Rescigno, C. W. McCurdy, and A. E. Orel, Extensions of the complex-coordinate method to the study of resonances in many-electron systems, Phys. Rev. A **17**, 1931 (1978).

[45] A. F. White, M. Head-Gordon, and C. W. McCurdy, Complex basis functions revisited: Implementation with applications to carbon tetrafluoride and aromatic N-containing heterocycles within the static-exchange approximation, J. Chem. Phys. **142**, 054103 (2015).

[46] F. Matz and T.-C. Jagau, Channel-specific core-valence projectors for determining partial Auger decay widths, Mol. Phys. , e2105270 (2022).

[47] F. Matz and T.-C. Jagau, Molecular Auger decay rates from complex-variable coupled-cluster theory, J. Chem. Phys. **156**, 114117 (2022).

[48] A. I. Krylov, Equation-of-motion coupled-cluster methods for open-shell and electronically excited species: The hitchhiker's guide to Fock space, Annu. Rev. Phys. Chem. **59**, 433 (2008).

[49] W. Skomorowski and A. I. Krylov, Feshbach-Fano approach for calculation of Auger decay rates using equation-of-motion coupled-cluster wave functions. II. Numerical examples and benchmarks, J. Chem. Phys. **154**, 084125 (2021).

[50] Florian Matz, Jonas Nijssen, and Thomas Jagau, Ab initio investigation of the auger spectra of methane, ethane, ethylene, and acetylene, (2023).

[51] V. Parravicini and T.-C. Jagau, Interatomic and intermolecular Coulombic decay rates from equation-of-motion coupled-cluster theory with complex basis functions, (2023), submitted; https://arxiv.org/abs/2305.10186.

[52] J. P. Drennhaus, A. Ferino-Pérez, F. Matz, and T.-C. Jagau, Coupled-cluster approach to Coster-Kronig decay and Auger decay in hydrogen sulfide and argon, arXiv preprint arXiv:2402.17368 (2024).

[53] A. Ferino-Pérez and T.-C. Jagau, Ab initio computation of Auger decay in heavy metals: Zinc about it, J. Phys. Chem. A (2024).

[54] N. K. Jayadev, A. Ferino-Pérez, F. Matz, A. I. Krylov, and T.-C. Jagau, The Auger spectrum of benzene, J. Chem. Phys. **158**, 064109 (2023).

[55] R. Spohr, T. Bergmark, N. Magnusson, L. O. Werme, C. Nordling, and K. Siegbahn, Electron spectroscopic investigation of Auger processes in bromine substituted methanes and some hydrocarbons, Phys. Scr. **2**, 31 (1970).

[56] E. E. Rennie, B. Kempgens, H. M. Köppe, U. Hergenhahn, J. Feldhaus, B. S. Itchkawitz, A. L. D. Kilcoyne, A. Kivimäki, K. Maier, M. N. Piancastelli, M. Polcik, A. Rüdel, and A. M. Bradshaw, A comprehensive photoabsorption, photoionization, and shake-up excitation study of the C1s cross section of benzene, J. Chem. Phys. **113**, 7362 (2000).

[57] S. Carniato, P. Selles, A. Ferté, N. Berrah, A. H. Wuosmaa, M. Nakano, Y. Hikosaka, K. Ito, M. Žitnik, K. Bučar, K. Soejima, K. Jänkälä, D. Cubaynes, J.-M. Bizau, L. Andric, M. A. Khalal, J. Palaudoux, P. Lablanquie, and F. Penent, Single photon simultaneous K-shell ionization/excitation in C_6H_6: Experiment and theory, J. Phys. B **53**, 244010 (2020).

[58] P. U. Manohar and A. I. Krylov, A non-iterative perturbative triples correction for the spin-flipping and spin-conserving equation-of-motion coupled-cluster methods with single and double substitutions, J. Chem. Phys. **129**, 194105 (2008).

[59] P. U. Manohar, J. F. Stanton, and A. I. Krylov, Perturbative triples correction for the equation-of-motion coupled-cluster wave functions with single and double substitutions for ionized states: Theory, implementation, and examples, J. Chem. Phys. **131**, 114112 (2009).

[60] D. A. Matthews and J. F. Stanton, A new approach to approximate equation-of-motion coupled cluster with triple excitations, J. Chem. Phys. **145**, 124102 (2016).

[61] T. C. Jagau, Non-iterative triple excitations in equation-of-motion coupled-cluster theory for electron attachment with applications to bound and temporary anions, J. Chem. Phys. **148**, 024104 (2018).

[62] R. Sarangi, M. L. Vidal, S. Coriani, and A. I. Krylov, On the basis set selection for calculations of core-level states: Different strategies to balance cost and accuracy, Mol. Phys. **118**, e1769872 (2020).

[63] M. L. Vidal, M. Epshtein, V. Scutelnic, Z. Yang, T. Xue, S. R. Leone, A. I. Krylov, and S. Coriani, The interplay of open-shell spin-coupling and Jahn-Teller distortion in benzene radical cation probed by x-ray spectroscopy, J. Phys. Chem. A **124**, 9532 (2020).

[64] E. Epifanovsky, A. T. B. Gilbert, X. Feng, J. Lee, Y. Mao, N. Mardirossian, P. Pokhilko, A. F. White, M. P. Coons, A. L. Dempwolff, Z. Gan, D. Hait, P. R. Horn, L. D. Jacobson, I. Kaliman, J. Kussmann, A. W. Lange, K. U. Lao, D. S. Levine, J. Liu, S. C. McKenzie, A. F. Morrison, K. D. Nanda, F. Plasser, D. R. Rehn, M. L. Vidal, Z.-Q. You, Y. Zhu, B. Alam, B. J. Albrecht, A. Aldossary, E. Alguire, J. H. Andersen, V. Athavale, D. Barton, K. Begam, A. Behn, N. Bellonzi, Y. A. Bernard, E. J. Berquist, H. G. A. Burton, A. Carreras, K. Carter-Fenk, R. Chakraborty, A. D. Chien, K. D. Closser, V. Cofer-Shabica, S. Dasgupta, M. de Wergifosse, J. Deng, M. Diedenhofen, H. Do, S. Ehlert, P.-T. Fang,

S. Fatehi, Q. Feng, T. Friedhoff, J. Gayvert, Q. Ge, G. Gidofalvi, M. Goldey, J. Gomes, C. E. González-Espinoza, S. Gulania, A. O. Gunina, M. W. D. Hanson-Heine, P. H. P. Harbach, A. Hauser, M. F. Herbst, M. Hernández Vera, M. Hodecker, Z. C. Holden, S. Houck, X. Huang, K. Hui, B. C. Huynh, M. Ivanov, Á. Jász, H. Ji, H. Jiang, B. Kaduk, S. Kähler, K. Khistyaev, J. Kim, G. Kis, P. Klunzinger, Z. Koczor-Benda, J. H. Koh, D. Kosenkov, L. Koulias, T. Kowalczyk, C. M. Krauter, K. Kue, A. Kunitsa, T. Kus, I. Ladjánszki, A. Landau, K. V. Lawler, D. Lefrancois, S. Lehtola, R. R. Li, Y.-P. Li, J. Liang, M. Liebenthal, H.-H. Lin, Y.-S. Lin, F. Liu, K.-Y. Liu, M. Loipersberger, A. Luenser, A. Manjanath, P. Manohar, E. Mansoor, S. F. Manzer, S.-P. Mao, A. V. Marenich, T. Markovich, S. Mason, S. A. Maurer, P. F. McLaughlin, M. F. S. J. Menger, J.-M. Mewes, S. A. Mewes, P. Morgante, J. W. Mullinax, K. J. Oosterbaan, G. Paran, A. C. Paul, S. K. Paul, F. Pavošević, Z. Pei, S. Prager, E. I. Proynov, Á. Rák, E. Ramos-Cordoba, B. Rana, A. E. Rask, A. Rettig, R. M. Richard, F. Rob, E. Rossomme, T. Scheele, M. Scheurer, M. Schneider, N. Sergueev, S. M. Sharada, W. Skomorowski, D. W. Small, C. J. Stein, Y.-C. Su, E. J. Sundstrom, Z. Tao, J. Thirman, G. J. Tornai, T. Tsuchimochi, N. M. Tubman, S. P. Veccham, O. Vydrov, J. Wenzel, J. Witte, A. Yamada, K. Yao, S. Yeganeh, S. R. Yost, A. Zech, I. Y. Zhang, X. Zhang, Y. Zhang, D. Zuev, A. Aspuru-Guzik, A. T. Bell, N. A. Besley, K. B. Bravaya, B. R. Brooks, D. Casanova, J.-D. Chai, S. Coriani, C. J. Cramer, G. Cserey, A. E. DePrince, R. A. DiStasio, A. Dreuw, B. D. Dunietz, T. R. Furlani, W. A. Goddard, S. Hammes-Schiffer, T. Head-Gordon, W. J. Hehre, C.-P. Hsu, T.-C. Jagau, Y. Jung, A. Klamt, J. Kong, D. S. Lambrecht, W. Liang, N. J. Mayhall, C. W. McCurdy, J. B. Neaton, C. Ochsenfeld, J. A. Parkhill, R. Peverati, V. A. Rassolov, Y. Shao, L. V. Slipchenko, T. Stauch, R. P. Steele, J. E. Subotnik, A. J. W. Thom, A. Tkatchenko, D. G. Truhlar, T. Van Voorhis, T. A. Wesolowski, K. B. Whaley, H. L. Woodcock, P. M. Zimmerman, S. Faraji, P. M. W. Gill, M. Head-Gordon, J. M. Herbert, and A. I. Krylov, Software for the frontiers of quantum chemistry: An overview of developments in the Q-Chem 5 package, J. Chem. Phys. **155**, 084801 (2021).

[65] A. I. Krylov and P. M. W. Gill, Q-Chem: An engine for innovation, WIREs: Comput. Mol. Sci. **3**, 317 (2013).

[66] R. S. Mulliken, Report on notation for the spectra of polyatomic molecules, J. Chem. Phys. **23**, 1997 (1955).

[67] Depending on molecular orientation, symmetry labels corresponding to the same orbital or

vibrational mode may be different. Q-Chem's standard molecular orientation is different from that of Mulliken.[66] For example, Q-Chem would place water molecule in the xz plane instead of the yz. Consequently, for C_{2v} symmetry, b_1 and b_2 labels are flipped. More details can be found at http://iopenshell.usc.edu/resources/howto/symmetry/. To avoid confusion with different molecular orientations and relabeling the states, here we report the structures and symmetry labels following the Q-Chem's notations.

[68] K. D. Nanda, M. L. Vidal, R. Faber, S. Coriani, and A. I. Krylov, How to stay out of trouble in RIXS calculations within the equation-of-motion coupled-cluster damped response theory? Safe hitchhiking in the excitation manifold by means of core-valence separation, Phys. Chem. Chem. Phys. **22**, 2629 (2020).

[69] K. D. Nanda, M. L. Vidal, R. Faber, S. Coriani, and A. I. Krylov, Correction: "How to stay out of trouble in RIXS calculations within the equation-of-motion coupled-cluster damped response theory? Safe hitchhiking in the excitation manifold by means of core-valence separation", Phys. Chem. Chem. Phys. **22**, 17749 (2020).

[70] S. A. Mewes, F. Plasser, A. Krylov, and A. Dreuw, Benchmarking excited-state calculations using exciton properties, J. Chem. Theory Comput. **14**, 710 (2018).

[71] F. Plasser, A. I. Krylov, and A. Dreuw, libwfa: Wavefunction analysis tools for excited and open-shell electronic states, WIREs: Comput. Mol. Sci. **12**, e1595 (2022).

[72] D. Menzel, G. Rocker, H.-P. Steinrück, D. Coulmanand P. A. Heimann, W. Huber, P. Zebisch, and D. R. Lloyd, Core excitation, decay, and fragmentation in solid benzene as studied by x-ray absorption, resonant Auger, and photon stimulated desorption, J. Chem. Phys. **96**, 1724 (1992).

[73] M. Epshtein, V. Scutelnic, Z. Yang, T. Xue, M. L. Vidal, A. I. Krylov, S. Coriani, and S. R. Leone, Table-top X-ray spectroscopy of benzene radical cation, J. Phys. Chem. A **124**, 9524 (2020).

[74] D. A. Little and J. Tennyson, An R-matrix study of singlet and triplet continuum states of N_2, J. Phys. B **47**, 105204 (2014).

[75] M. Klinker, C. Marante, L. Argenti, J. González-Vázquez, and F. Martín, Electron correlation in the ionization continuum of molecules: Photoionization of N_2 in the vicinity of the hopfield series of autoionizing states, J. Phys. Chem. Lett. **9**, 756 (2018).

[76] J. Creutzberg, W. Skomorowski, and T.-C. Jagau, Computing decay widths of autoionizing rydberg states with complex-variable coupled-cluster theory, J. Phys. Chem. Lett. **14**, 10943 (2023).

[77] K. Ueda, M. Okunishi, H. Chiba, Y. Shimizu, K. Ohmori, Y. Sato, E. Shigemasa, and N. Kosugi, Rydberg-valence mixing in the C 1s excited states of CH_4 probed by electron spectroscopy, Chem. Phys. Lett. **236**, 311 (1995).

[78] M. Neeb, A. Kivimäki, B. Kempgens, H.M. Köppe, and A.M. Bradshaw, The C 1s auger decay spectrum of CF_4: an analysis of the core-excited states, J. Phys. B **30**, 93 (1997).

[79] L. Ungier and T. D. Thomas, Near threshold excitation of KVV Auger spectra in carbon monoxide using electron–electron coincidence spectroscopy, J. Chem. Phys. **82**, 3146 (1985).

[80] Florian Matz, private communication.

[81] N. K. Jayadev, W. Skomorowski, and A.I. Krylov, Molecular-orbital framework of two-electron processes: Application to Auger and intermolecular Coulomb decay, J. Phys. Chem. Lett. **14**, 8612 (2023).